CHARACTERISATION OF CRUDE OILS AND THEIR FOULING DEPOSITS

Andrew Young*[1], Silvia Venditti[2], Cesur Berrueco[2], Mengyan Yang[1]
Andrew Waters[1], Haddy Davies[1], Simon Hill[1], Marcos Millan[2] and Barry Crittenden[1]

[1]Department of Chemical Engineering, University of Bath, Bath, UK, BA2 7AY
[2]Department of Chemical Engineering, Imperial College London, UK, SW7 2AZ

*corresponding author: ay211@bath.ac.uk

ABSTRACT

A small (1 litre) batch stirred cell system has been developed to study crude oil fouling at surface temperatures up to 400°C and pressures up to 30 bar. Fouling resistance-time data are obtained from experiments in which the principal operating variables are surface shear stress, surface temperature, heat flux and crude oil type. The oils and deposits are characterised and correlated with the experimental heat transfer fouling data to understand better the effects of process conditions such as surface temperature and surface shear stress on the fouling process. Deposits are subjected to a range of qualitative and quantitative analyses in order to gain a better insight into the crude oil fouling phenomenon. Thermal data which can be obtained relatively quickly from the batch cell provide fouling rates, Arrhenius plots, apparent activation energies and fouling threshold conditions as a function of process variables. The data also contribute to existing knowledge about the compensation plot.

INTRODUCTION

Various methods have been adopted to study the complex problem of fouling in crude oil preheat exchangers. Research using actual plant data is slow, subject to a variety of logistical and operational requirements which do not lend themselves well to fundamental scientific studies (Crittenden et al., 1992), and can create difficulties in the interpretation of the thermal data (Takemoto et al., 1999). A number of laboratory methods have been developed to study liquid phase fouling (Epstein, 1981; Chenoweth, 1988) including for crude oils use of the stirred batch cell (Eaton and Lux, 1984), or use of a recycle flow loop with either a tubular cross section (eg Crittenden et al., 2009) or an annular cross section (eg Wilson and Watkinson, 1995; Bennett et al., 2009).

Whilst laboratory studies can eliminate the principal practical disadvantages of studying fouling on refinery exchangers they, in turn, introduce their own disadvantages, the principal one being that the crude oil is not exposed to the time-temperature-flow history of the crude in the oil refinery. Accordingly, concerns are that crucial fouling precursors might become depleted in extended running of both batch cells and recycle flow loops, and that flow structures are not typical of industrial practice. Nevertheless, laboratory-scale studies can be made with precise operating conditions and can provide excellent access to the heat transfer surface, its deposits and the fluids from which the fouling originates. Laboratory-scale methods also allow study of the effects of the heat transfer surface (its material, morphology, enhancement, etc) as well as devices which might be used to simultaneously improve heat transfer and reduce fouling (eg Crittenden et al., 1993).

In the current research a batch stirred cell has been designed to operate under conditions close to those found in crude oil preheat trains, namely a maximum pressure of 30 bar and a maximum surface temperature of around 400°C. The cell design following closely that of Eaton and Lux (1983, 1984) was chosen since it offers extraordinary flexibility. Crude oils can be changed easily, as can the fouling fluid chemistry (eg by adding asphaltenes, metal salts, etc). The cell can be sparged with various gases, eg oxygen and nitrogen, and the heat transfer surface is easily inspected and changed. Computational fluid dynamics (CFD) software also allows the thermal and fluid flow characteristics of the complex batch stirred cell geometry to be predicted and validated (Yang et al., 2009a).

APPARATUS AND EXPERIMENTAL METHOD

Apparatus

The general arrangement of the cell is shown in Fig. 1. The cell comprises a pressure vessel made in-house from a block of 304 stainless steel together with a top flange. The base of the vessel houses an upwards pointing test probe heated internally by a cartridge heater, the heat flux from which is controlled electrically (Fig. 2). The crude oil (≈ 1.0 litre) is agitated by a downwards facing cylindrical stirrer mounted co-axially with the test probe and driven by an electric motor via a magnetic drive. External band heaters are incorporated to provide initial heating to the vessel and its contents. An internal cooling coil uses a non-fouling fluid (Paratherm) to remove heat at the rate that it is inputted via the cartridge heater during the fouling run. The vessel is fitted with a pressure relief valve and there is a single thermocouple to measure the crude oil bulk temperature.

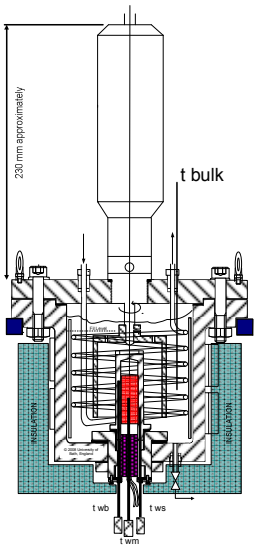

Fig. 1 The batch stirred cell

Heated test probes are manufactured in-house from low carbon steel with a material specification similar to that of a standard A179 heat exchanger tube. Each probe fits tightly over the cartridge heater supplied by Watlow Ltd. A coherent light scanning probe (Scantron Industrial Products, Taunton, England) is used to obtain the initial surface roughness R_a. Three test probes have been made (denoted A, B and C). Probes A and B have relatively high R_a values of ≈10μm. Probe C had a similar surface characterization to that of a standard mild steel heat exchanger tube (A179). Three small diameter type J thermocouples (supplied by TC Thermocouples Ltd) located at various heights within the walls of the test probe are used to follow progress of the fouling at different axial locations. The three thermocouples are labeled *twb*, *twm* and *tws*, their positions being shown in Fig. 2. Pressure is maintained by means of a nitrogen blanket. Air can be admitted to sparge the crude oil in advance of a fouling run if so desired. Heat is ultimately dissipated to atmosphere from the Paratherm by means of an air-cooled heat exchanger.

Experimental Method

The vessel is initially filled with the specimen crude oil. For most experiments, the oil is then sparged with air at 1 bar whilst being stirred with the desired experimental agitation speed for 30 minutes. The fully aerated vessel is then purged and blanketted with nitrogen at 20 bar. The vessel and its contents are then brought up to the bulk operating temperature by means of the external band heaters. The heating ramp is normally 15°C/min.

At 200°C the stirrer is started and heating with the band heaters is continued until the desired bulk temperature (typically around 260°C) is reached. Once the desired bulk temperature is reached power is applied to the cartridge heater to provide the desired heat flux or desired surface temperature, as appropriate. Also at this point the controlled cooling circuit is established to develop a steady-state heat transfer rate in the cell. Control of the steady-state heat transfer conditions is achieved with a bespoke combination of band heating and cooling coil operation under traditional PID control.

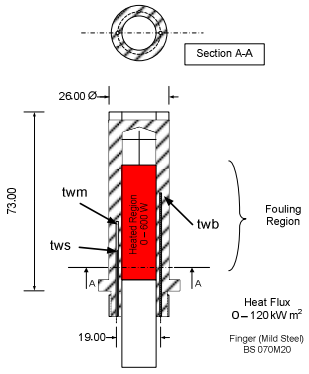

Fig. 2 Heated test probe

At the end of an experiment the power to the cartridge heater is switched off, the stirrer speed is reduced and the vessel is allowed to cool down by maintaining the flow through the cooling coil. The test probe and cartridge heater assembly can then be removed from the base of the batch cell once it has been drained so that the test probe can be removed for inspection and deposit characterization. An example of a deposit on a heated test probe is shown in Fig. 3.

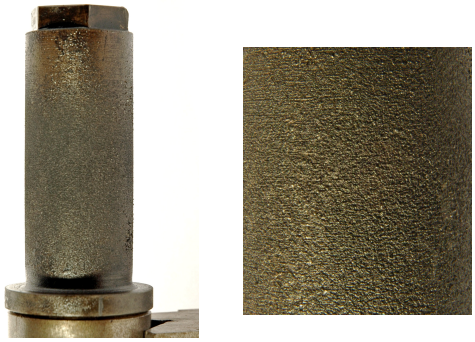

Fig. 3 Deposit on a heated probe

If a previously fouled probe is to be used for a subsequent run it is thoroughly cleaned by brushing in the following sequence of solvents: ethanol, kerosene, *para*-xylene and acetone.

Fouling Resistance and Fouling Rate Calculations

The fouling resistance R_f is calculated from Eq. (1) (Crittenden et al., 1987; Bennett et al., 2009).

$$R_f = \left(\frac{T_s - T_b}{q}\right)_t - \left(\frac{T_s - T_b}{q}\right)_{t=0} \quad (1)$$

Here, q is the heat flux and T_s and T_b are the local surface and bulk temperatures at time t and time zero, respectively. This equation avoids the need to calculate film heat transfer coefficients. The cell was operated at constant q and constant T_b and so Eq. (1) becomes:

$$R_f = \left(\frac{T_{st} - T_{so}}{q} \right) \quad (2)$$

Here, T_{st} and T_{so} are the surface temperatures at time t and zero, respectively. In the cell, measurements are made of temperatures within the probe wall (*twb*, *twm* and *tws* of Fig. 2). CFD is used to convert these temperatures to those at the actual metal surface/crude oil interface (Yang et al., 2009a). Provided that the film heat transfer coefficient does not alter as fouling proceeds, then the initial interfacial temperature remains constant throughout a fouling run (Crittenden and Alderman, 1988). From Eq. (2), the instantaneous rate of fouling is now proportional to the rate at which the local surface temperature changes with time.

Crude Oils

Table 1 summarises the principal properties of three crude oil blends tested in the cell to date. Analyses were provided by LGC Ltd (Teddington, UK). Crudes A and B are untreated raw blends of sour crudes blended in the suppliers' laboratory. Crude DS is a desalted blend.

Table 1 Properties of crude oil blends tested

	Crude A	Crude B	Crude DS
API	27.5	24.43	30.92
Viscosity (cst) @ 80 ^oC	15	8.8	2.9
Viscosity (cst) @ 260 ^oC	1.74	0.745	0.58
Total Sulphur (% wt)	2.82	3.65	2.1
Iron (ppm)	4	4	1
Nickel (ppm)	42	25	18
Vanadium (ppm)	226	52	55
Saturates (%)	28.36	21.68	29.2
Aromatics (%)	56.87	65.63	63.65
Resins (%)	6.8	5.68	4.28
Asphaltenes (%; IP143)	8	7	2.87
CII	0.56	0.4	0.48

A more complete analysis of metals present in Crudes A and B both before and after fouling experiments were made using ICP-MS by LGC Ltd. The comparisons are shown in Table 2. All concentrations are in mg/kg. The data show that the only significant elements present are nickel, sulphur, iron and vanadium. For both crudes it could be inferred that nickel and vanadium take no role in the fouling process unless they act as catalysts. The increase in iron concentration for Crude A and the high levels of sulphur are addressed later in the paper.

Using the standard contact test BS EN828 (1998) the critical surface tension was found to be about 30 mN/m for the surface of test probe C. The data to determine the critical contact angle are shown in Figure 4.

Table 2 Element concentrations in the crude oils tested

Analysis	Crude A		Crude B	
	before	after	before	after
Silver	4	<2	<2	<2
Aluminium	<1	<5	<1	<1
Boron	<2	<2	<2	<2
Barium	<1	<1	<1	<1
Calcium	<2	<2	<2	<1
Chromium	<1	<1	<1	<1
Copper	<1	<1	2	<1
Iron	<1	23	4	2
Potassium	<2	<2	<2	<2
Magnesium	<2	<2	<2	<2
Manganese	<1	<1	<1	<1
Molybdenum	3	<5	<1	<1
Sodium	<10	<2	<2	<2
Nickel	46	47	25	26
Phosphorus	<2	<2	<2	<2
Lead	<2	<2	<2	<2
Sulphur	28,000	27,800	36,500	37,000
Silicon	<1	<1	5	<1
Tin	<2	<1	<1	<1
Titanium	<1	<1	<1	<1
Vanadium	230	241	52	57
Zinc	<1	<1	<1	<1

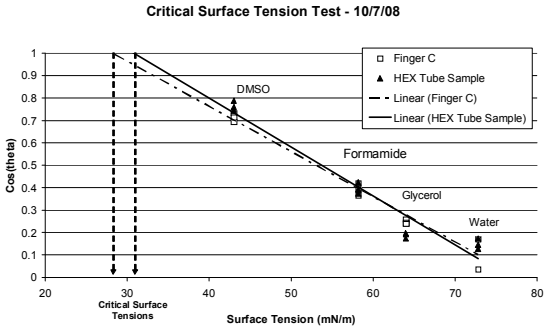

Fig. 4 Critical surface tension test

RESULTS

To date the batch stirred cell has been used not only to determine the effects of principal operational parameters such as surface temperature, bulk temperature and shear stress on fouling rates but also to determine some deposit and fluid characteristics as fouling proceeds.

Deposit Distribution and Morphology

There are two reasons why the deposit is not uniformly distributed over the axial length of the probe (Fig. 3). Firstly, the heated section of the cartridge heater does not extend to the ends of the probe. Secondly, the flow patterns near the end of the probe are quite complex, especially near the bottom. Hence, distributions of shear stress, surface temperature and heat flux over the cell's probe surface are modelled for each fouling experiment using the Comsol CFD package (Yang et al., 2009a). For any given agitation speed, bulk temperature and heat flux, the surface stress is found to be virtually constant along the surface of the probe

except for a reduction at the very bottom (Yang et al., 2009a). The CFD simulation results are validated against the measured temperature data at various axial positions within the probe (Yang et al., 2009a).

After a fouling run, the cell is drained of crude oil, dismantled and the probe removed. After drying in a vacuum oven overnight at 100°C, the deposit thickness along and around the probe is measured using a laser and coherent light scanning procedure (Proscan 2000, Scantron Industrial Products Ltd, Taunton, UK). An example screen-shot of a Proscan 2000 surface profile is shown in Fig. 5, the peak deposit thickness being about 15 µm.

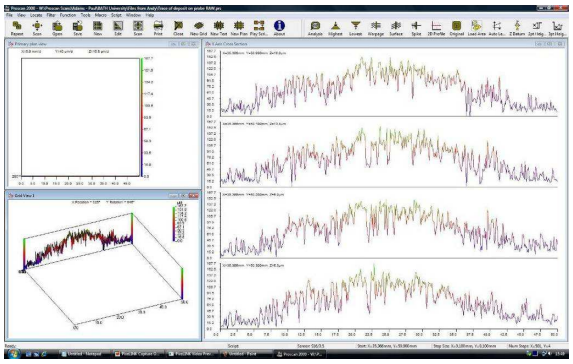

Fig. 5 Example Proscan deposit thickness profile

The deposit thickness profile along the heated surface reveals a maximum near the middle of the heated test probe surface. The CFD-predicted surface temperature profiles are strikingly similar in shape (Yang et al., 2009a). This resemblance between deposit thickness and surface temperature profiles is to be expected since the effect of surface temperature on a crude oil fouling rate is strong (Crittenden et al., 2009). It is now possible to correlate, for a fixed surface shear stress, the local fouling rate against the local surface temperature, and hence to obtain an Arrhenius plot from a single experimental run (Yang et al., 2009a). Since the shear stress can be varied by changing the speed of rotation of the cell's cylindrical stirrer, the effect of shear stress on fouling behaviour can be studied as well.

Fouling Resistance and Rate

In virtually all experiments to date, the fouling resistance has been found to vary linearly with time (eg Fig. 6). An induction period is usually seen when a well-cleaned probe is used. Conversely, an induction period is not normally observed when a test probe is left in situ in the cell between runs. A relatively simple lumped parameter model has been developed to account for the growth in fouling resistance including the induction period (Yang et al., 2009b). The fouling rate used in all Arrhenius plot calculations is that after completion of the induction period.

Photomicrographs and Scanning Electron Microscopy

Figure 7 shows a photomicrograph of a deposit formed from Crude DS (not sparged with air) at a surface temperature of 380°C, bulk temperature of 280°C, heat flux of 110 kW/m^2 and stirrer speed of 100 rpm. The photograph was taken at the location of thermocouple *twb*. It is clear that the deposit surface is rough, in accordance qualitatively with the scan shown in Fig. 5.

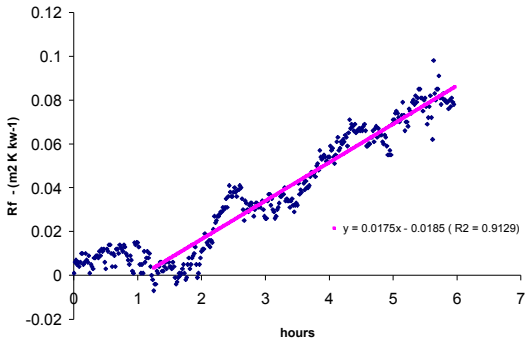

Fig. 6 Typical fouling curve for Crude B

Fig. 7 Photomicrograph of deposit from Crude DS

Figure 8 shows the test probe fitted with a small coupon removeable for inspection by scanning electron microscopy. The SEM picture shown in Fig. 9 reveals that the deposit formed on the surface is striated in a manner very similar to that found previously by Wilson and Watkinson (1995, 1996) in their hydrocarbon autoxidation fouling studies. The individual particle sizes seen in Fig. 9 seem to be of the order of 100 µm.

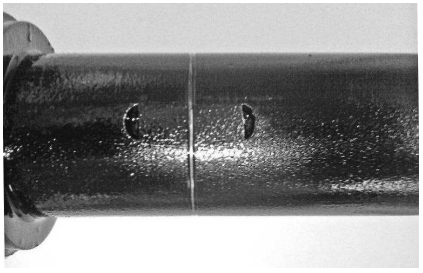

Fig. 8 Probe fitted with test coupon held by a thin wire

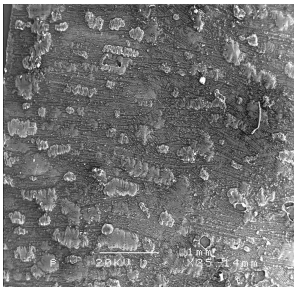

Fig. 9 SEM of test coupon surface
(the white line represents 1 mm length)

Thermogravimetric Analysis

Thermogravimetric analysis (TGA) in nitrogen/air was carried out at Imperial College London on a deposit obtained in the batch stirred cell with Crude B. Prior to TGA, the deposit was dried overnight in a vacuum oven at 100°C in an attempt to remove as much free crude oil as possible. As can be seen in Fig. 10, the deposit lost an appreciable weight (about 27%) as the temperature was ramped from about 200 to 450°C. Almost certainly this loss was due to the removal of free crude oil up to a temperature which was not too far above the maximum surface temperature the deposit experienced in the batch cell.

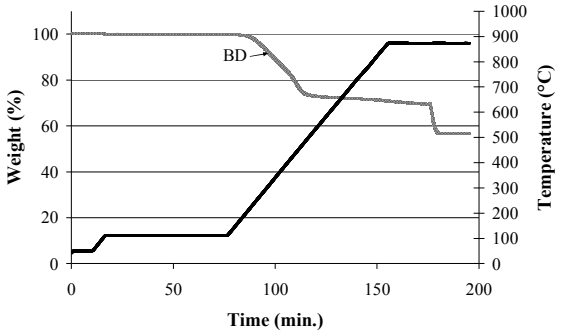

Fig. 10 TGA analysis of deposit from Crude B

A further weight loss (about 4%) occurred as the temperature was ramped further from 450 to 870°C, which was almost certainly due to pyrolysis of the deposit. Finally, air was introduced into the apparatus to burn remaining combustible elements (about 13%) and the final weight was that of the ash in the deposit, namely about 56%.

Size Exclusion Chromatography and UV-Fluorescence

An initial characterisation of deposit samples by chromatography did not show significant differences between them and the feed material. This led to the use of different solvents to fractionate the sample in order to make the identification easier via the isolation of different classes of compounds. Deposit samples were separated into heptane-soluble (HS) and heptane-insoluble (HI) fractions. Solubility in the mixture NMP/CHCl3 (6:1) was finally estimated due to the use of this eluent in the SEC system. Only the soluble fraction of the samples is analysed by this technique. Results are shown in Table 3. The observed changes in the solubility class of significant amounts of material strongly suggest that chemical reactions are taking place within these samples. Overall, Table 3 shows decreasing proportions of HI-material in the BPost sample (1.8 %) in comparison with the feed crude, BPre (8.61 %) as the deposit precipitated. It is also interesting to note the high percentage of HI in the deposits recovered (84 %).

Table 3 Solubility test results for Crude B

Solubility (%)	BPre	BD	BPost
HS	90.8	16	98
HI	8.61	84	1.8
$NMP/CHCl_3$ (6:1)	-		-

Size exclusion chromatography (SEC) and UV-fluorescence tests were carried out with the details being reported by Venditti et al. (2009). Fig. 11 presents size exclusion chromatograms of the deposits using Crude oil B, allowing for a comparison between retention times of the main eluted peaks and the corresponding samples. There are slight differences between the crude used (BPre) and the deposits obtained (BD). This fact justifies the use of heptane to fractionate deposits into heptane-soluble (HS) and heptane-insoluble (HI) fractions (16% and 84%, respectively) with the attempt of isolating heavy material. As expected, there was a shift to shorter elution times (greater masses) between the deposit (BD) and the HI fraction, suggesting the presence of larger molecules in the HI sample. The maximum intensity of the peak of material resolved by column porosity was found to have shifted by about two minutes, which corresponds to a difference of about 200 u between the deposit and its HI fraction, as calculated using the PAHs calibration (Berrueco et al., 2008).

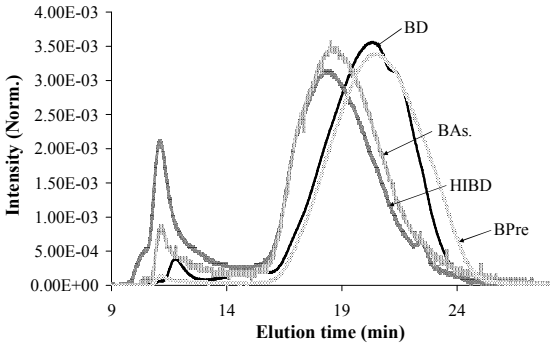

Fig. 11 Size exclusion chromatograms for Crude B

In addition, the HI fraction of the deposit was compared with asphaltenes (BAs.) extracted from the same crude oil, which are, by definition, heptane-insoluble/toluene soluble. SEC results show similarities in terms of molecular mass distribution. The corresponding UV-F results indicate that the biggest polynuclear aromatic systems are present in the

HI-fraction. This is consistent with the larger molecular mass material observed by SEC. In addition, it is relevant to note that the HI fraction of the deposits shows the size of chromophores broadly similar to those from asphaltene extracted from the same crude.

Elemental Analyses

Elemental analyses were made by Medac Ltd (Egham, UK) and Imperial College. The mass data of Table 4 reveal that deposits formed from both crude oils contained significant quantities of sulphur and iron suggesting the formation of iron sulphide, as discussed by Watkinson (2004). The atomic H:C ratios were almost identical for the two crudes at 1.37 for Crude A and 1.36 for Crude B.

Table 4 Elemental analyses of deposits (Medac)

Element	C	H	N	S	Fe
Crude A	36.12	4.11	<0.1	16.61	13.71
Crude B	53.98	6.11	0.48	13.82	7.53

The elemental analyses in Table 5 indicate a composition mainly based on carbon and minor N content. The results also indicate a higher content of sulphur (22.22%) and iron (26.87%) for the deposit (BD) in comparison with those of feed material (BPre). Iron is almost certainly due to corrosion reactions, whilst sulphur probably originates from the crude oil itself. Corrosion products are confirmed by the high value of ash content (56%). 12 % of fixed carbon is related to the short period of exposure at high temperature in comparison with the heat exchanger deposits. This factor depends on the operating conditions at the laboratory scale.

Table 5 Ultimate and proximate analyses of deposit from Crude B (Imperial College)

(% wt.)	BPre	BD	BAs.
C	84.34	29.22	85.44
H	11.48	3.37	7.76
N	0.88	0.16	0.83
S	2.6	22.22	4.83
Fe	4 (ppm)	26.87	-
H/C atomic ratio	1.62	1.37	1.08
C/S atomic ratio	0.011	0.28	0.021
Ash	-	56	-

X-ray Diffraction Analysis

The XRD data shown in Fig. 12 for a deposit formed from Crude B reveals the presence of iron and sulphur in addition to carbon. Bearing in mind that the peak height for sulphur is expected to be higher than that for iron in XRD, Fig. 12 lends further support to the probability of iron sulphide formation. Hence, it is quite possible that the fouling process from this crude oil is related to iron sulphide corrosion of the heat transfer surface which might help to explain why preliminary experimental work on the batch stirred cell failed to produce any measurable fouling even at quite high surface temperatures. That is, the role of sulphur present in a crude oil (Tables 1 and 2) might be crucial to the first fouling of the test probes.

Effect of Shear Stress

The shear stress at the surface of the heated probe was determined using CFD (Yang et al., 2009a). The stirred cell flow structure becomes turbulent at relatively low cell Reynolds numbers (Smith and Townsend, 1982; Mullin et al., 1983).

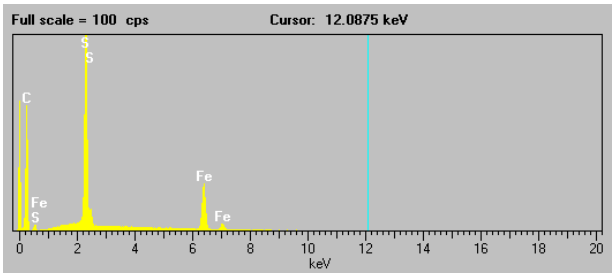

Fig. 12 XRD analysis of a deposit formed from Crude B

For refinery applications, the relationship between the stirred cell Reynolds number and the tubular flow Reynolds number which gives the same surface shear stress is shown in Fig. 13. Here, the tube internal diameter was 14.8 mm and the crude oil viscosity and density were 0.0008 Pa s and 760 kg/m^3, respectively. The stirred cell Reynolds number is defined by $Re = \rho N D^2/\mu$ where N is the rotational speed of the stirrer of diameter D, and μ and ρ are the viscosity and density of the bulk crude oil, respectively.

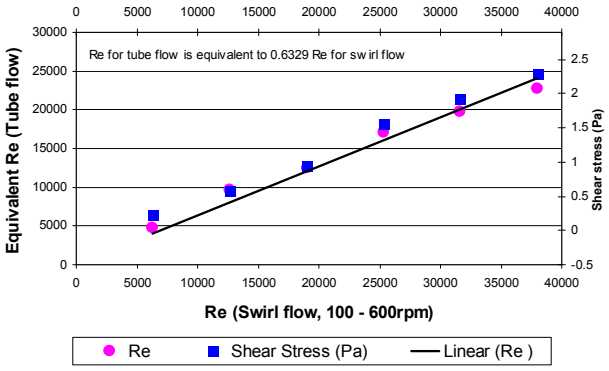

Fig. 13 Equivalent Reynolds numbers

The effect of stepping up for a short period the stirrer speed and hence the shear stress on the fouling rate of Crude B is shown in Fig. 14. This shows that the fouling rate for all the three probe thermocouple locations was constant over a three hour period when the surface shear stress was kept constant at 0.75 Pa. The stirrer speed was then increased from 200 rpm to 550 rpm such that the surface shear stress was increased to 2.5 Pa for a short period of time. The stirrer speed was then reduced back to 200 rpm such that the surface shear stress was reduced back to its original value of 0.75 Pa. Fig. 14 shows that the fouling rates more-or-less

resumed their original values, albeit at somewhat lower fouling resistances. The results from this experiment provide evidence therefore that an increase in surface shear stress can lead to the removal of a crude oil fouling deposit.

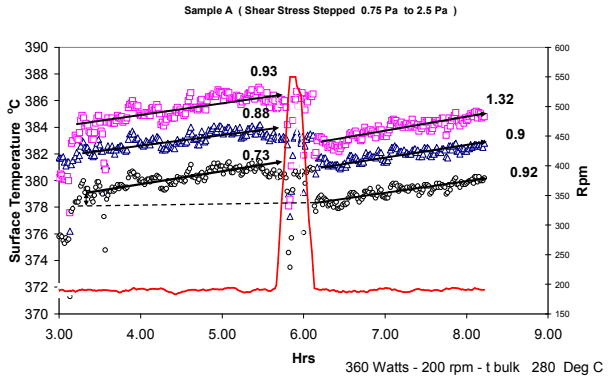

Fig. 14 Effect of stirrer speed and hence of shear stress

Effect of Surface Temperature

The stirred cell can also be used to show how the surface temperature affects the fouling rate. Preliminary experiments had shown that the batch stirred cell could be used to obtain a long-time fouling run by shutting down the apparatus overnight and resuming the experiment later on without cleaning the test probe surface. No changes in fouling rates were found by operation in this manner provided that the same stirrer speed and cartridge heater power were used. This property of the system was then exploited in the study of the effect of surface temperature.

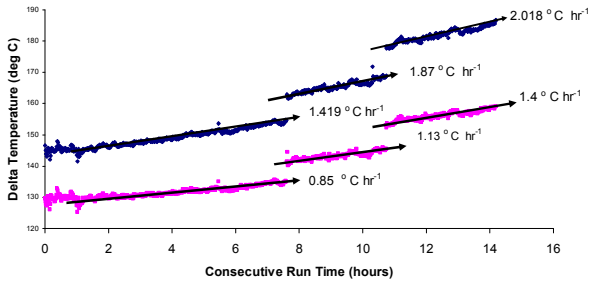

Fig. 15 Effect of changing cartridge power for Crude B

For a given stirrer speed the surface temperature can be changed quickly by changing the power supplied to the cartridge heater. This change manifests itself in a change in the difference between the probe and bulk temperatures. Figure 15 shows such changes for Crude B stirred at 200 rpm. The initial values of *twb* and *tws* were 390°C and 380°C, respectively. It can be seen that the probe-bulk temperature difference increases with an increase in power supplied. It can also be seen that the fouling rate (which is proportional to the slope of the temperature difference plot) increases as well, as expected.

Figure 16 shows the change in probe temperatures (*twb*, *twm* and *tws*) as a function of the cumulative run time for Crude A for a fixed stirrer speed of 100 rpm. Six runs were carried out consecutively on the same test probe without cleaning in between runs.

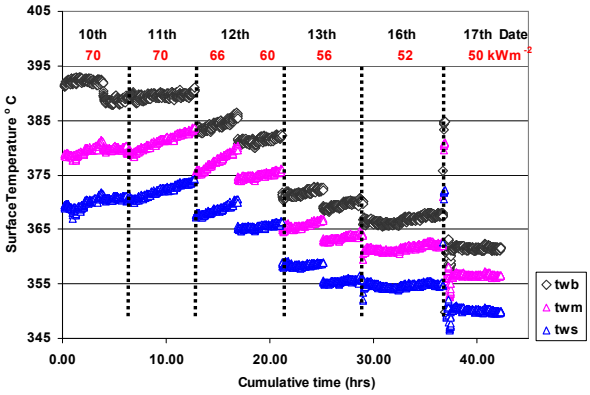

Fig. 16 Effect of surface temperature for Crude A

For the run on 11th Feb. 2009 the fouling rate for *twm* was 2.82×10^{-6} m^2K/kJ which compares well with rates found in other studies (Asomaning et al., 2000; Saleh et al., 2004). Between experiments, the power supplied to the cartridge heater was reduced, thereby lowering the surface temperatures. This experiment was repeated for stirrer speeds of 200 and 300 rpm. The general Arrhenius expression which relates the initial fouling rate to the surface temperature, pre-exponential factor and apparent activation energy is given by Eq. (3).

$$\left.\frac{dR_f}{dt}\right|_{t=0} = A\exp\left(-E_A/RT_{SO}\right) \qquad (3)$$

The Arrhenius plots obtained for the three stirrer speeds are shown in Fig. 17.

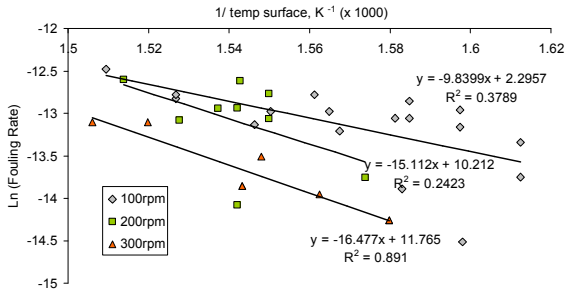

Fig. 17 Effect of stirrer speed on Arrhenius plot (Crude A)

It is clear that there is an increase in apparent activation energy E_A with stirrer speed, an effect which has been noted before with the effect of velocity (ie turbulence) on apparent

activation energy in a tubular recycle system (Crittenden et al., 2009).

Threshold Conditions

The ability to carry out experiments in the batch stirred cell by varying surface temperature at constant surface shear stress or by varying surface shear stress at constant surface temperature means that the fouling rate data can be plotted in such a way that it is possible to extrapolate back to find the point at which no fouling occurs. This is the fouling threshold. An example plot of fouling rate as a function of stirrer speed is shown in Fig. 18.

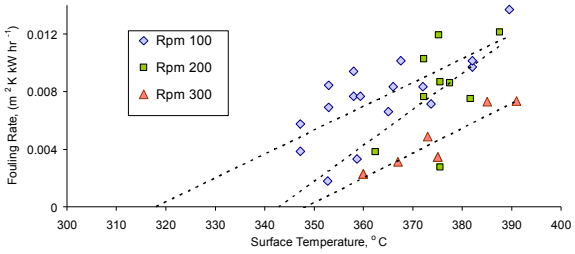

Fig. 18 Effect of stirrer speed on fouling rates (Crude A)

The data of Fig. 18 have been extrapolated linearly back to zero fouling resistance to find a relationship between surface temperature and stirrer speed at which there would be no fouling. The threshold conditions of temperature and related apparent activation energy are shown plotted against the equivalent tubular Reynolds number in Fig. 19 (dark squares = E_A; light diamonds = T_s). As expected, the threshold surface temperature is increased by operation at a higher shear stress (ie at a higher stirrer speed in the batch cell or a higher flow velocity in the equivalent tubular flow system). Figure 19 shows also that the relatively high apparent activation energy increases with the amount of surface shear. This phenomenon has been seen previously in fouling studies with styrene polymerization and Maya crude oil fouling in tubular recycle systems (Crittenden et al., 2009).

Compensation Plot

The relationship between the logarithm of the pre-exponential factor and the apparent activation energy of an Arrhenius plot forms the basis of the compensation plot (Bennett et al., 2009; Crittenden et al., 2009). The equation of the compensation plot is given by Eq. (4) where a is the gradient and b is the intercept (Crittenden et al., 2009).

$$\ell n\, A = aE_A + b \qquad (4)$$

Two types of compensation plot are suggested: a "true" one in which an isokinetic relationship occurs such as that found by Bennett et al (2009) who worked with Kuwaiti crude oils or a "false" one which is based on experimental conditions and the way in which the compensation plot is constructed.

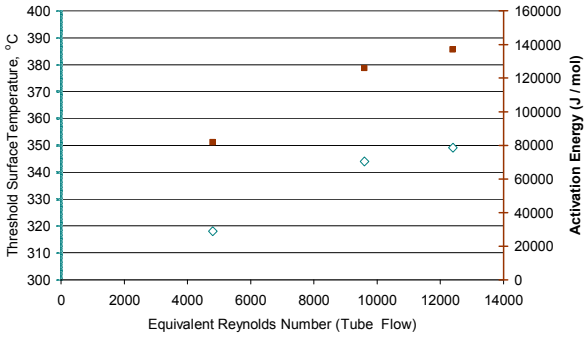

Fig. 19 Threshold plot for Crude A

Figure 20 shows the compensation plot for eight separate crude oil systems which include Crude A and Crude B. Whilst it might seem remarkable that all the data fall virtually on the same straight line, this plot almost certainly contains data from systems with both "true" and "false" types. The potential value of the compensation plot is described elsewhere (Crittenden et al., 2009).

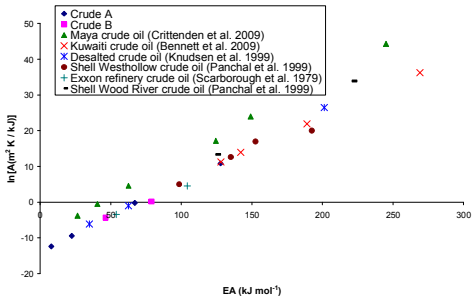

Fig. 20 Compensation plot for a range of crude oils

CONCLUSIONS

A batch cell stirred cell system has been developed which allows relatively fast studies to be made of the effect of key operating parameters on crude oil fouling and facilitates characterization of deposits formed and feedstocks used. The experimental system, supported by CFD studies, also allows fouling threshold conditions of surface temperature and shear stress to be identified relatively quickly in the laboratory. The system additionally is able to generate further data to be used in the construction of a generic compensation plot for all crude oils.

ACKNOWLEDGMENTS

The authors are grateful to the UK's Engineering and Physical Sciences Research Council (EPSRC) for the award of a research grant (EP/D506131/1) to study the role of asphaltenes in crude oil fouling. The authors are grateful also to their project partners at the University of Cambridge, and to ExxonMobil and Petronas for the supply of crude oils.

NOMENCLATURE

a gradient of linear plot of Eq. (4), mol/kJ
A pre-exponential factor in Arrhenius equation, m^2K/W
b intercept of linear plot of Eq. (4)
D stirrer diameter, m
E_A apparent activation energy, kJ/mol
N stirrer speed, Hz
q heat flux, kW/m^2
R gas constant, kJ/molK
R_a probe surface roughness, μm
Re batch stirred cell Reynolds number
R_f fouling resistance, m^2K/W
T_b bulk temperature, K
T_s surface temperature, K
T_{so} initial (clean) surface temperature, K
T_{st} surface temperature at time t, K
t time, h
μ viscosity, Pa s
ρ density, kg/m^3

REFERENCES

Asomaning, S., Panchal, C. B., and Liao, C. F., 2000, Correlating field and laboratory data for crude oil, *Heat Transfer Engineering*, Vol. 21 (3), pp. 17-23.

Bennett, C. A., Kistler, R. S., Nangia, K., Al-Ghawas, W., Al-Hajji, N. and Al-Jemaz, A., 2009, Observation of an isokinetic temperature and compensation effect for high temperature crude oil fouling, *Heat Transfer Engineering*, Vol. 30 (10-11), pp. 794-804.

Berrueco, C., Venditti, S., Morgan, T. J., Alvarez, P., Millan-Agorio, M., Herod, A. A. And Kandiyoti, R., 2008, Calibration of size-exclusion chromatography columns with 1-methyl-2-pyrrolidinone (NMP)/chloroform mixtures as eluent: applications to petroleum-derived samples, *Energy and Fuels*, Vol. 30 (10-11), pp. 3265-3274.

Chenoweth, J. M., 1988, Liquid fouling monitoring equipment, in *Fouling Science and Technology*, eds. L. F. Melo, T. R. Bott and C. A., Kluwer Academic Publishers, Dordrecht, pp. 49-65.

Crittenden, B. D., Hout, S. A. and Alderman, N. J., 1987, Model experiments of chemical reaction fouling, *TransIChemE Part A*, Vol. 65, pp. 165-170.

Crittenden, B. D. and Alderman, N. J., 1988, Negative fouling resistances: the effect of surface roughness, *Chemical Engineering Science*, Vol. 43, pp. 829-838.

Crittenden B. D., Kolaczkowski, S. T. and Downey, I. L., 1992, Fouling of crude oil preheat exchangers, *Trans IChemE Part A*, Vol. 70, pp. 547-557.

Crittenden, B. D., Kolaczkowski, S. T. and Takemoto, T., 1993, Use of in-tube inserts to reduce fouling from crude oils, *AIChE Symp Series*, Vol. 89, No. 295, pp. 300-307.

Crittenden, B. D., Kolaczkowski., S. T. and Phillips D. Z., 2009, Crude oil fouling in a pilot-scale parallel tube apparatus, *Heat Transfer Engineering*, Vol. 30 (10-11), pp. 777-785.

Eaton, P., 1983, Fouling test apparatus, US patent 4383438.

Eaton, P. and Lux, R., 1984, Laboratory fouling test for hydrocarbon feed-stocks, *ASME-HTD*, Vol. 35, pp. 33-42.

Epstein, N., 1981, Fouling in heat exchangers, in *Fouling of Heat Transfer Equipment*, eds. E. F. C. Somerscales and J. G. Knudsen, Hemisphere, Washington, pp 701-732.

Knudsen, J. G., Lin, D. C. and Ebert, W. A., 1997, The determination of the threshold fouling curve for a crude oil, *Proc. Int. Conference on Understanding Heat Exchanger Fouling and its Mitigation*, Castelvecchio Pas, Italy.

Mullin T., Lorenzen, A. and Pfister, G., 1983, Transition to turbulence in a non-standard rotating flow. *Physics Letters A* 96 (5), 236-238

Panchal, C. B., Kuru, W. C., Ebert, W. A., Liao, C. F. and Palen, J., 1999, Threshold conditions for crude oil fouling, *Proc. Int. Conference on Understanding Heat Exchanger Fouling and its Mitigation*, Castelvacchio Pas, Italy.

Saleh, Zaid S., Sheikholeslami, R. and Watkinson, A. P., 2004, Fouling characteristics of a light Australian crude oil, *Proc. 2003 ECI Conf. on Heat Exchanger Fouling and Cleaning: Fundamentals and Applications*, Sante Fe, New Mexico, pp. 226-233.

Scarborough, C. E., Cherrington, D. C., Diener, R. and Golan, L. P., 1979, Coking of crude oil at high heat flux levels, *Chem. Eng. Progress*, Vol. 75 (7), pp. 41-46.

Smith G P and Townsend A A, 1982, Turbulent couette flow between concentric cylinders at large Taylor numbers. *J. Fluid Mech.*, Vol 123, 187-217

Takemoto, T., Crittenden, B. D. and Kolaczkowski, S. T., 1999, Interpretation of fouling data in industrial shell and tube heat exchangers, *TransIChemE Part A*, Vol. 77, pp. 769-778.

Venditti, S., Berrueco, C., Alvarez, P., Morgan, T., Millan, M., Herod, A. A. and Kandiyoti, R., 2009 Developing characterisation methods for fouling deposited in refinery heat exchangers, accepted for inclusion in *Proc. Eurotherm Conference on Fouling and Cleaning in Heat Exchangers*, Schladming, Austria.

Watkinson, A. P., 2004, Chemical reaction fouling of organic fluids, *Chemical Engineering and Technology*, Vol. 15 (2), pp. 82-90.

Wilson, D. I. and Watkinson, A. P., 1995, Model experiments of autoxidation reaction fouling, *TransIChemE Part A*, Vol. 73, pp. 59-68.

Wilson, D. I. and Watkinson, A. P., 1996, A study of autoxidation fouling in heat exchangers, *Can. J. Chem. Eng.*, Vol. 74 (2), pp. 236-246.

Yang, M., Young, A. and Crittenden, B. D., 2009a, Use of CFD to correlate crude oil fouling against surface temperature and surface shear stress in a stirred fouling apparatus, accepted for inclusion in *Proc. Eurotherm Conference on Fouling and Cleaning in Heat Exchangers*, Schladming, Austria.

Yang, M., Young, A. and Crittenden, B. D., 2009b, Modelling of the induction period of crude oil fouling, accepted for inclusion in *Proc. Eurotherm Conference on Fouling and Cleaning in Heat Exchangers*, Schladming, Austria.